THE JOURNAL OF PHYSICAL CHEMISTRY B

Article

pubs.acs.org/JPCB

# Structure and Kinetics of Fatty Acid Langmuir Monolayers on Zinc Salt Solutions

Sophie Cantin,*[,†] Marie-Claude Fauré,[‡,§] Françoise Perrot,[†] and Michel Goldmann[‡,§]

[†]Laboratoire de Physicochimie des Polymères et des Interfaces (LPPI, EA 2528), Institut des Matériaux, Université de Cergy-Pontoise, 5 mail Gay-Lussac Neuville/Oise, 95031 Cergy-Pontoise Cedex, France

[‡]Institut des Nanosciences de Paris (INSP, UMR 7588), Université Pierre et Marie Curie, 4 place Jussieu, 75252 Paris Cedex 05, France

[§]UFR Faculté des Sciences Fondamentales et Biomédicales, Université Paris Descartes, 45 rue des St pères 75006 Paris, France

**ABSTRACT:** The adsorption of zinc cations under behenic acid Langmuir monolayers was investigated by means of isotherm measurements, grazing incidence X-ray diffraction and Brewster angle microscopy. The structure of the films was characterized as a function of $Zn^{2+}$ concentration, for three different counterions (chloride, iodide, bromide) and at two subphase pHs (5.5 and 7.5). At pH 5.5 and in the studied concentration range, $Zn^{2+}$ adsorption leads to a condensation of the fatty acid monolayer with the same phase transitions as over pure water. In contrast, at higher pH the organic X-phase is evidenced immediately above a concentration threshold without any ion organization. Even though $Cu^{2+}$ and $Zn^{2+}$cations induce both the fatty acid X-phase, the kinetics of its formation appears strongly different. Indeed, as for $Mg^{2+}$ and $Cd^{2+}$, the intermediate new I-structure is evidenced in the course of $Zn^{2+}$ adsorption although superstructures are observed only for $Mg^{2+}$ and $Cd^{2+}$. However, for $Zn^{2+}$, the I-phase evolves to the final state through a new structure called X′ and a continuous X′−X transition. Finally, any effect of the counterion is evidenced neither during the kinetic process nor in the final state.

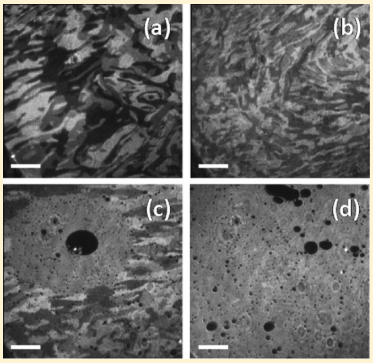


## INTRODUCTION

In many biological assemblies such as bones or shells, the nucleation and growth of a mineral layer is directed by an organic phase.[1] In view of the design of new biomimetic composite materials and for a better understanding of the interaction mechanisms involved in such architectures, intensive research is carried out on model organic−inorganic systems. In particular, Langmuir monolayers of amphiphilic molecules at the surface of aqueous solution of metal ions allow a systematic study of the mineralization processes.[2−8] In this case, the physicochemical parameters (pH, temperature) as well as the organic and inorganic compounds can be easily tuned. In addition, specific powerful techniques are available to characterize the structure of the systems, like grazing incidence X-ray diffraction (GIXD) and brewster angle microscopy (BAM). In the case of fatty acids as organic template that allow mimicking the acidic residues predominant in proteins present in biominerals, unexpected modifications of organic monolayer structures may be induced by the adsorption of divalent cations, even for very dilute solutions.[3,9−11] Indeed, provided that the fatty acid chain is long enough or the temperature sufficiently low, cations like $Cd^{2+}$, $Mg^{2+}$, $Mn^{2+}$, and $Pb^{2+}$ self-organize on a monatomic superlattice of the hexagonal distorted fatty acid unit cell. The strong organic−inorganic interaction induces at null surface pressure a new condensed chiral fatty acid structure, not observed in the pure water phase diagram. Above a concentration threshold that depends on the cation and the pH, the superstructure occurs "immediately", as evidenced by coupling GIXD measurements, BAM observations, and surface pressure−molecular area isotherms.[12,13] Below this threshold, the superstructure formation follows a kinetic process in which time scale is controlled by the number of cations per fatty acid headgroup. In the presence of $Cd^{2+}$ and $Mg^{2+}$, the kinetics involves an intermediate weakly ordered organic phase called "I-phase" not observed over pure water.[12,13] The initial fatty acid $L_2$-phase evidenced over divalent cation-free subphase evolves to the superstructure via the I-phase through two successive first-order phase transitions.

The other divalent metal ions, such as $Ba^{2+}$, $Co^{2+}$, $Zn^{2+}$, $Cu^{2+}$, and $Ca^{2+}$, only lead to a condensation of the fatty acid monolayer into either the usual high surface pressure S-phase or a new structure called the X-phase without any ion ordering.[9,14−16] The X-phase observed in the presence of $Zn^{2+}$, $Cu^{2+}$, ans $Ca^{2+}$ is a highly distorted hexagonal structure highlighting the strong interaction of the fatty acid headgroups with these cations. The kinetics of the X-phase formation has been studied in the case of $Cu^{2+}$ cations.[15] In contrast to the cations forming a superstructure, no intermediate I-phase was detected during the adsorption and the initial $L_2$-phase evolves directly to the X-phase.

In addition, the subphase pH, that is, the initial ionization state of the fatty acid headgroups, plays a significant role in the

**Received:** July 16, 2013
**Revised:** November 21, 2013
**Published:** November 27, 2013

**Table 1. Summary of the Different Phases and Phase Transitions Evidenced during Adsorption of Several Divalent Cations under a Behenic Acid Monolayer**

| divalent cation | | initial state | phase transition order | intermediate state(s) | phase transition order | final structure |
|---|---|---|---|---|---|---|
| $Cd^{2+}$ | pH 7.5[a] | $L_{2h}$-phase | 1st order | I-phase | 1st order | superstructure (chiral organic phase) |
| $Mg^{2+}$[b] | pH 5.5 | $L_{2h}$-phase | 1st order | I-phase | 1st order | superstructure (chiral organic phase) |
| | pH 10.5 | $L_{2h}$-phase | 1st order | $L'_2$-phase $\xrightarrow{\text{1st order}}$ I-phase | 1st order | superstructure (chiral organic phase) |
| $Cu^{2+}$[c] | pH 5.5 | $L_{2h}$-phase | 2nd order | X-like phase | 2nd order | X-phase |
| | pH 7.5 | $L_{2h}$-phase | 1st order | X-like phase | 2nd order | X-phase |
| $Zn^{2+}$ | pH 7.5 | $L_{2h}$-phase | 1st order | I-phase $\xrightarrow{\text{1st order}}$ X′-phase | 2nd order | X-phase |

[a]Reference 12. [b]Reference 13. [c]Reference 15.

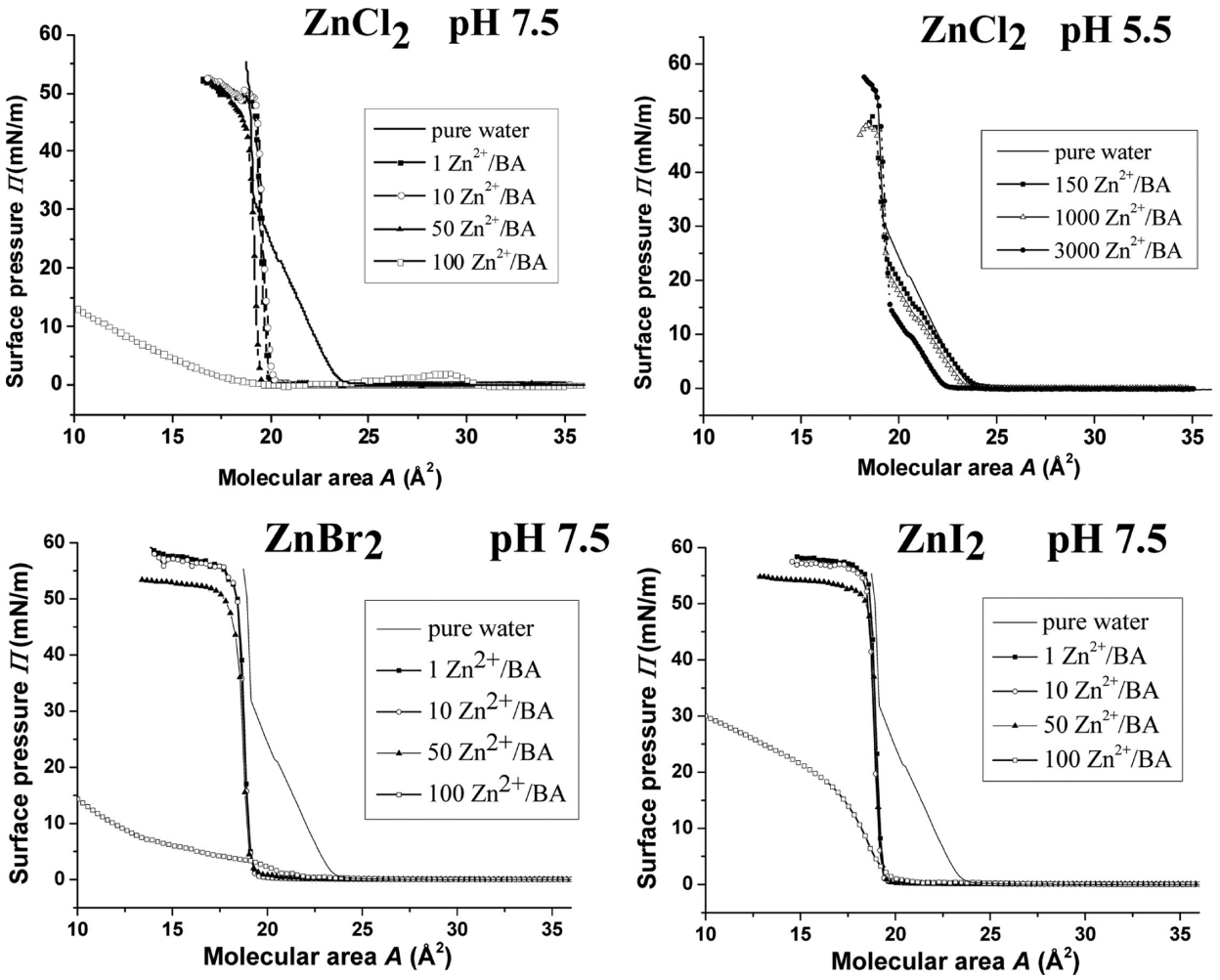


**Figure 1.** Surface pressure versus mean molecular area isotherms for BA monolayers spread over different aqueous solutions of $Zn^{2+}$ ions and at different $Zn^{2+}$ concentrations (broken lines). The concentration is indicated as a number of $Zn^{2+}$ ions per BA molecule. (a) $ZnCl_2$ solutions adjusted to pH 7.5, (b) $ZnCl_2$ solutions adjusted to pH 5.5, (c) $ZnI_2$ solutions adjusted to pH 7.5, and (d) $ZnBr_2$ solutions adjusted to pH 7.5.

structures observed during cation adsorption. Moreover, polarization-modulated infrared reflection−absorption spectroscopy experiments indicate that the gap between the interfacial pH and the subphase pH strongly depends on the cation nature.[17] However, GIXD characterization shows that the final structure (superstructure or X-phase) is independent of the pH whereas the sequence of phases leading to this final state may depend on the pH. Indeed, when $Mg^{2+}$ cations are dissolved in the subphase, one observes an additional stage in the sequence of phases at pH 10.5 with respect to pH 5.5. This stage is associated to a fatty acid monolayer condensation toward the $L'_2$-phase.[13] In the case of $Cu^{2+}$cations that induce the X-phase, the pH induces a difference in the order nature of the phase transition from the $L_2$-phase to the X-phase. Indeed, this transition is first order at pH 7.5 while it is second order at pH 5.5.[15] Table 1 summarizes the sequence of phases evidenced during the adsorption of the different studied divalent cations.

Adsorption kinetics of monovalent or divalent cations at charged surfaces has been previously described using the Poisson−Boltzmann−Stern equations; however, such a model cannot bring information about the organic−inorganic in-plane structures, and until now the reasons why some cations lead to a defined superstructure are still fuzzy.[18] In addition, the exact


dx.doi.org/10.1021/jp407047a | J. Phys. Chem. B 2013, 117, 16275−16282

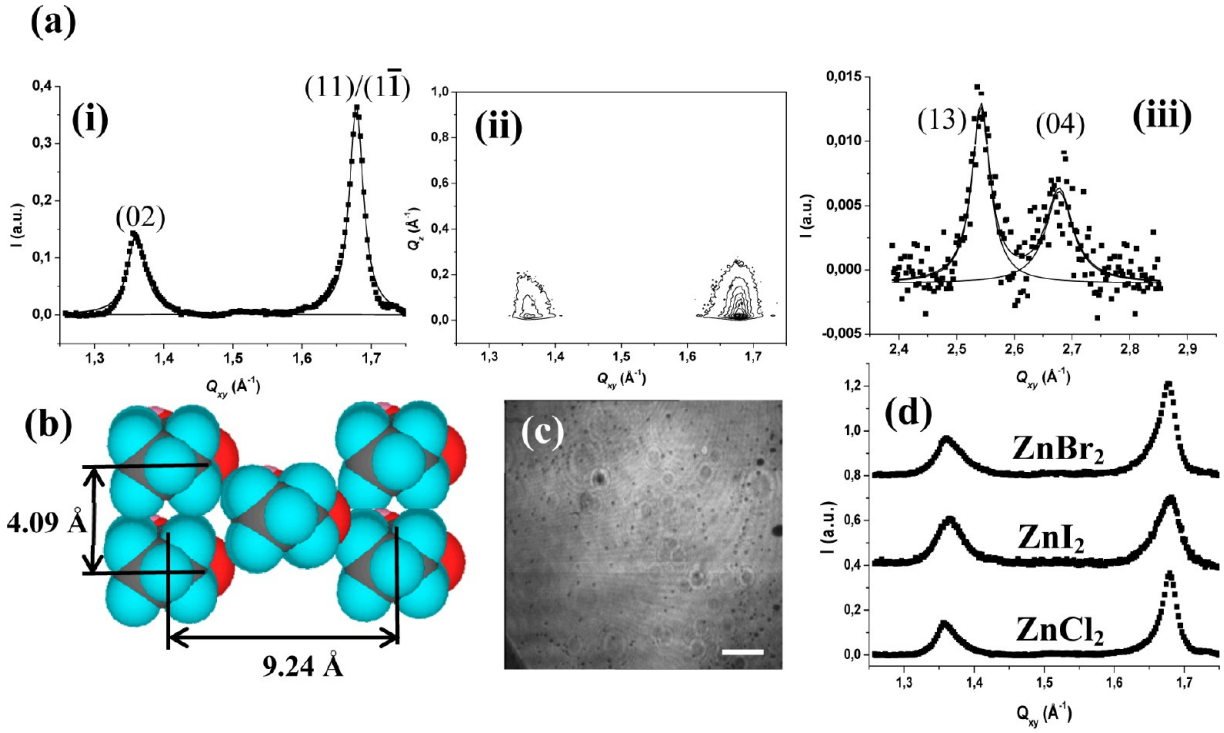


**Figure 2.** X-ray diffraction data for a BA monolayer spread over a $Zn^{2+}$ solution of 100 $Zn^{2+}$ ions/BA molecule concentration, adjusted to pH 7.5. The surface pressure of the monolayer is $\Pi = 0$ mN/m. (a) In the presence of chloride as counterion; integrated diffracted intensity versus $Q_{xy}$ values in the $Q_{xy}$ ranges, respectively, 1.25−1.75 Å$^{-1}$ (i) and 2.35 − 2.95 Å$^{-1}$ (iii) and contours of equal intensity versus $Q_{xy}$ and $Q_z$ in the $Q_{xy}$ range 1.25−1.75 Å$^{-1}$ (ii). (b) Scheme of the possible organization of the BA molecules within the X-phase rectangular cell. (c) BAM image obtained with an analyzer in the presence of chloride as counterion. The white bar represents 100 $\mu$m. (d) Scan of intensity as a function of $Q_{xy}$ integrated over all $Q_z$ values in the presence of chloride, iodide, or bromide as counterion.

chemical composition of the crystalline lattice remains unknown. In the case of $Pb^{2+}$, X-ray absorption fine structure spectroscopy (XAFS) characterizations suggest that the adsorbed species are more likely hydrolysis products rather than individual ions.[19] More recently, the location of $Mn^{2+}$ and $Mg^{2+}$ ions in the superlattices was achieved using crystallographic tools to analyze GIXD data. The deduced organization of the ions as clusters suggests the presence of hydrolyzed species.[11]

In this paper, we focus on behenic acid (BA) Langmuir monolayers spread over salt solutions of zinc at room temperature and at different concentrations. Two subphase pHs, 5.5 and 7.5, were investigated. These values are below and above fatty acid p$K_a$ in order to change the initial ionization state of the headgroups. First surface pressure-molecular area isotherms were measured for BA over $ZnCl_2$ solutions as a function of the concentration. BAM observations and structural characterizations by GIXD were performed. The role of the counterion was also examined by replacing chloride by iodide or bromide. In the case of $Zn^{2+}$ cations, previous studies were performed by using acetate as counterion.[16] Finally, kinetic studies of the X-phase formation were performed. GIXD and BAM measurements were thus conducted below the concentration threshold at which the X-phase is immediately observed, in order to determine the sequence of phases leading to this final state.

## II. EXPERIMENTAL SETUP AND MATERIALS

Behenic acid (BA, $CH_3$-$(CH_2)_{20}$-COOH) (Sigma, purity >99%) was first dissolved in chloroform (Merck, analytical grade) to a concentration of 0.389 g·L$^{-1}$. The monolayer was then spread over $ZnCl_2$, $ZnI_2$, or $ZnBr_2$ (Sigma, purity 99.99%) solutions prepared with ultrapure deionized water from a Milli-Q Millipore system. The subphase pH was either unadjusted (5.5) or adjusted to 7.5 with $NaHCO_3$ (Sigma).The temperature was set to 20 °C using a water refrigerated/heating circulator.

After film deposition, the mean molecular area was 37 Å$^2$. For GIXD or BAM studies, the monolayer was then compressed to a mean molecular area of 22 Å$^2$ corresponding to a surface pressure of 0 mN/m.

The surface pressure-molecular area isotherms were performed on a Nima Langmuir trough (Nima, 601BAM).

Grazing incidence X-ray diffraction experiments were carried out at the BW 1 beamline of the Hasylab facility. The experimental setup has been previously described.[13] The trough was moved by 2 mm horizontally after each scan avoiding the monolayer degradation due to X-ray exposure but limiting the number of scans on the same film.

Brewster angle microscopy observations were carried out on a home-built experiment.[20] The 600 $\mu$m × 600 $\mu$m large images were obtained with a spatial resolution close to 2 $\mu$m.

The Langmuir trough geometry (volume $V$, surface $S$) was different for each experimental setup: $V$ = 367 mL, $S$ = 324 cm$^2$ for BAM experiments, $V$ = 250 mL, $S$ = 450 cm$^2$ for GIXD, and $V$ = 305 mL, $S$ = 518 cm$^2$ for isotherm measurements. Consequently, in order to ensure time coherence between all these experiments we used an experimental unit expressing the salt concentration as a number of $Zn^{2+}$ ions per behenic acid molecule.[12]


dx.doi.org/10.1021/jp407047a | J. Phys. Chem. B 2013, 117, 16275−16282

## III. RESULTS AND DISCUSSION

**A. Characterization of BA Monolayers over $ZnCl_2$ Solutions at pH 7.5.** *a. Surface Pressure − Molecular Area Isotherms.* Figure 1a presents the surface pressure−molecular area isotherms obtained for BA Langmuir monolayers spread over chloride salt solutions of zinc adjusted to pH 7.5 at different $Zn^{2+}$ concentrations. The number of $Zn^{2+}$ ions per BA molecule was varied between about $13 \times 10^{-2}$ and 3000, corresponding to a concentration range between $10^{-7}$ and $3 \times 10^{-3}$ mol·L$^{-1}$. The isotherm measured over pure water at the same pH is also shown for comparison. Even at very low $Zn^{2+}$ ion concentrations ($10^{-6}$ mol·L$^{-1}$), a strong condensation of the BA monolayer is evidenced and the $L_2$-phase detected over pure water is no longer observed. From the slope of the isotherms at low surface pressure (between 2 and 15 mN/m), one can determine the monolayer compressibility. It decreases from 6.4 m·N$^{-1}$ over pure water ($L_2$-phase compressibility) to 0.7 m·N$^{-1}$ over $ZnCl_2$ solutions, independently of the concentration in the range 1−50 $Zn^{2+}$ ions per BA molecule. This value is close to the one measured in the usual high surface pressure S-phase,[21,22] meaning that low $Zn^{2+}$ concentrations have a significant effect on the monolayer rigidity. This is confirmed by the significant modification of the isotherm shape at higher $Zn^{2+}$ concentrations. Indeed, above a concentration threshold close to 100 $Zn^{2+}$ ions/BA molecule, the strong rigidity of the film leads to erroneous surface pressure measurements, as the Wilhelmy paper of the pressure sensor is kept prisoner in the monolayer. Such particular isotherm shape was previously evidenced for BA Langmuir monolayers spread over chloride salt solutions of $Cu^{2+}$ above a concentration threshold for immediate X-phase formation, in the same way as in the presence of the superstructures formed by $Cd^{2+}$, $Mg^{2+}$, $Mn^{2+}$, and $Pb^{2+}$.[10,15] $Zn^{2+}$ ions seem to induce a similar behavior on the BA monolayer with a monolayer condensation at low ion concentration followed by the appearance of a very rigid film at higher concentration. One can notice that the corresponding concentration threshold is a factor 20 higher for $Zn^{2+}$ than for $Cu^{2+}$. This could arise from variations in the interfacial pH depending on the cation added in the subphase.[17] Indeed, PM-IRRAS experiments indicate that the balance between dissociated and undissociated molecules depends on the divalent cation.

The solid line in each figure represents isotherm for BA monolayer, measured on divalent cation−free subphase at the same pH.

*b. GIXD and BAM Observations of the Final State.* BA monolayers spread over $ZnCl_2$ solutions adjusted to pH 7.5 were then characterized by GIXD. The molecular area was set to $A$ = 22 Å$^2$ and different subphase concentrations were investigated. Above the concentration threshold evidenced by means of isotherms at 100 $Zn^{2+}$ ions/BA, the diffraction spectra are independent of the concentration. As shown in Figure 2a for a concentration of 100 $Zn^{2+}$ ions/BA, two in-plane first order diffraction peaks are detected at $Q_{xy}$ = 1.360 Å$^{-1}$ and $Q_{xy}$ = 1.678 Å$^{-1}$, indicating a distorted hexagonal lattice. The contours of equal intensity as a function of $Q_{xy}$ and $Q_z$ show that these peaks are not symmetrical, which could mean that the transition is not completely achieved (Figure 2a). However, higher concentrations lead to the same diffraction spectra. The peak positions are similar to those reported for heneicosanoic acid monolayers spread over a $5 \times 10^{-4}$ M Zn acetate solution at a temperature of 10 °C.[16] No peak corresponding to inorganic compounds is detected. The diffraction patterns are characteristic of the fatty acid X-phase where the peaks are respectively assigned to the nondegenerate (02) and the degenerate (11) and (1$\bar{1}$) Bragg reflections in terms of the rectangular unit cell. This indexation, opposite compared to the S-phase, is confirmed by the observation of two not previously reported second order peaks at $Q_{xy}$ = 2.538 Å$^{-1}$ and $Q_{xy}$ = 2.673 Å$^{-1}$ (Figure 2a) and corresponding to the (13) and (04) Bragg reflections. The deduced rectangular lattice parameters are $a$ = 4.09 Å, $b$ = 9.24 Å, leading to a molecular area $A$ = 18.9 Å$^2$. These values can be compared to the cell parameters and molecular area corresponding to a herringbone packing (HB) of the backbone planes of the molecules ($a$ = 5.0 Å, $b$ = 7.5 Å, $A$ = 18.7 Å$^2$) and a pseudoherringbone (PHB) structure ($a$ = 4.4 Å, $b$ = 8.7 Å, $A$ = 19.1 Å$^2$). These two structures correspond to the denser chain packing ordering evidenced in the condensed phases of fatty acids and alcohols Langmuir monolayers.[23] In the HB cell, the angle $\alpha$ between the backbone planes of the central molecule in the unit cell and the molecules at the corners is 90°, whereas in the PHB cell this angle is 40°. The cell of the X structure formed in presence of $Zn^{2+}$ is strongly elongated, much more than the X-phase cell evidenced in the presence of $Cu^{2+}$cations in the subphase ($a$ = 4.27 Å, $b$ = 8.97 Å).[15] This strong distortion means that $\alpha$ should be lower than 40°. Considering the structure of a behenic acid molecule and the cell dimensions, the carbon backbone planes of the molecules at the corners of the cell lie probably nearly parallel to the $b$ axis (Figure 2b) and the structure appears thus closer to a PHB packing than the HB one.

By fitting the peaks with Lorentzian shapes, the positional correlation length $L$ can be deduced from the full width at half-maximum (fwhm) according to $L = 2/\text{fwhm}$. One obtains $L^{02}$ = 200 Å and $L^{11}$ = 250 Å, respectively, in the (02) and (11)/(1$\bar{1}$) directions. These values are significantly lower than those obtained for the X-phase induced by $Cu^{2+}$ ions adsorption ($L^{02}$ = 425 Å and $L^{11}$ = 330 Å).[15] This could be related to the slight asymmetry of the peaks.

The X-phase was then observed by BAM at a molecular area $A$ = 22 Å$^2$ with an analyzer on the path of the reflected light. Because of the distortion of the unit cell, an optical anisotropy resulting from the presence of domains with different lattice orientations could be observed. However, independently of the subphase concentration above 100 $Zn^{2+}$ ions per BA, no optical anisotropy was detected in the condensed phase, in contrast to the X-phase domains formed when $Cu^{2+}$ cations are dissolved in the subphase (Figure 2c).[15] This probably indicates that the size of the crystallites is smaller than the microscope resolution (2 $\mu$m).

**B. Effect of the Subphase pH and Role of the Counterion.** The adsorption of $Zn^{2+}$ ions under BA monolayers was then investigated at a subphase pH of 5.5 for different $ZnCl_2$ subphase concentrations (Figure 1b). Even at the highest studied concentrations ($3 \times 10^{-3}$ mol·L$^{-1}$ or 3000 $Zn^{2+}$/BA, the ions being no longer soluble at higher concentration) and unlike the results at pH 7.5, one observes the same phases' succession as over pure water ($L_2$−$L'_2$−S). Nevertheless, the surface pressures at which they occur decrease with increasing ion concentration. $Zn^{2+}$ ions thus only seem to have a condensing effect on the BA monolayer. Quite similar condensation was previously reported for a stearic acid monolayer spread over $ZnCl_2$ solutions at pH 6.8.[24]

For $CuCl_2$ solutions, it was previously shown that the X-phase is also formed at pH 5.5 above a concentration threshold


dx.doi.org/10.1021/jp407047a | J. Phys. Chem. B 2013, 117, 16275−16282

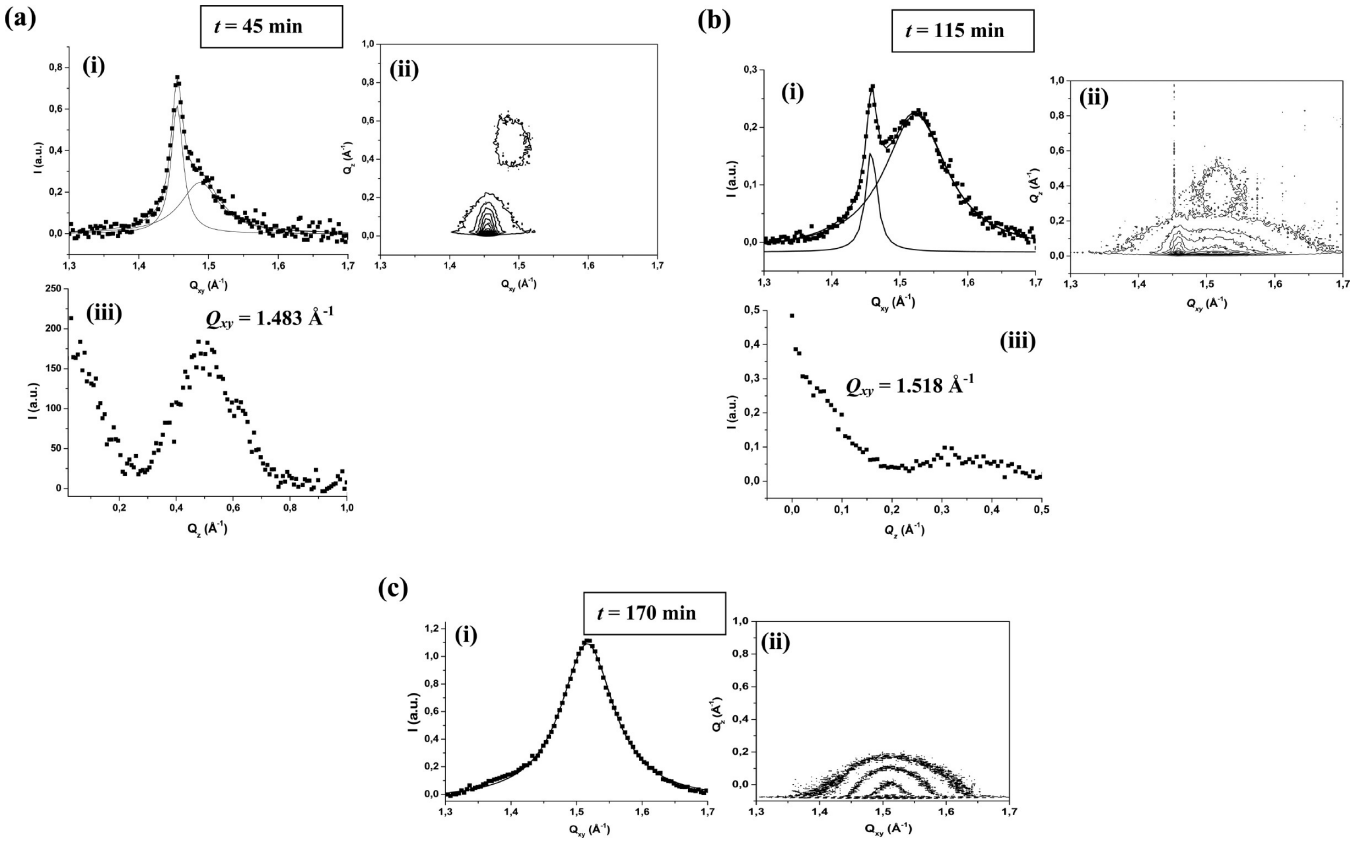


**Figure 3.** Time evolution of the X-ray diffraction pattern obtained for a BA monolayer over a $ZnCl_2$ solution of 1 $Zn^{2+}$ ions/BA molecule concentration, adjusted to pH 7.5. The surface pressure of the monolayer is $\Pi$ = 0 mN/m. (a) $t$ = 45 min: $L_{2h}$-phase. (i) Scan of intensity as a function of $Q_{xy}$ integrated over all $Q_z$ values. (ii) Contours of equal intensity versus the in-plane and out-plane scattering vector components $Q_{xy}$ and $Q_z$. (iii) $(11)/(1\bar{1})$ rod scan of intensity at $Q_{xy}$ = 1.483 $Å^{-1}$ as a function of $Q_z$. (b) $t$ = 115 min: $L_{2h}$-I phase transition. (i) Scan of intensity as a function of $Q_{xy}$ integrated over all $Q_z$ values. (ii) Contours of equal intensity versus $Q_{xy}$ and $Q_z$ values, showing the coexistence of a broad in-plane peak with the $L_{2h}$ phase out-of-plane $(11)/(1\bar{1})$ peak at $Q_{xy}$ = 1.518 $Å^{-1}$. (iii) Rod scan of intensity at $Q_{xy}$ = 1.518 $Å^{-1}$ as a function of $Q_z$ supporting these coexistence. (c) $t$ = 170 min: I-phase. (i) Scan of intensity as a function of $Q_{xy}$ integrated over all $Q_z$ values. (ii) Contours of equal intensity versus the in-plane and out-plane scattering vector components $Q_{xy}$ and $Q_z$.

close to 100 $Cu^{2+}$ ions per BA molecule, that is, a factor of 20 higher than the one obtained at pH 7.5.[15] As the concentration threshold at pH 7.5 is significantly higher for $Zn^{2+}$ than for $Cu^{2+}$ (100 $Zn^{2+}$/BA, 5 $Cu^{2+}$/BA), one can expect that decreasing the pH implies that in the studied concentration range, the X-phase could be no longer reachable due to $Zn^{2+}$solubility limit. At pH 5.5, the fatty acid headgroups are not ionized at the beginning of the ion adsorption and the ionization state changes in the course of cation adsorption. As a result, a larger amount of cations is necessary to bring the monolayer into the X-phase.

The role of the counterion was then studied by replacing chloride by iodide or bromide. The isotherms measured as a function of the ion concentration at a subphase pH of 7.5 are shown in Figure 1c,d. The isotherm networks are similar to the one obtained in the presence of chloride with a condensation of the BA monolayer at low concentration and a drastic change of the isotherm shape above a concentration threshold estimated to 100 $Zn^{2+}$ ions per BA molecule. The value of the threshold is thus the same as for $ZnCl_2$ solutions. GIXD measurements were then performed above the concentration threshold (Figure 2d). The diffraction peaks characteristics of the X-phase are also detected at exactly the same position indicating that the counterion does not play any significant role in the formed structure in this case.

**C. Study of the Kinetic Process.** The kinetics of the X-phase formation at pH 7.5 was then studied at $Zn^{2+}$ concentrations below the threshold and in the presence of the three different counterions, chloride, iodide, and bromide. The evolution with time of the BA monolayer was investigated by means of BAM and GIXD. Only the time scale of the kinetic process was modified according to cation concentration, without any change in the sequence of phases. In addition, no difference was evidenced between the evolutions observed in the presence of chloride, iodide and bromide as counterions.

Results of GIXD measurements (Figures 3 and 4) and BAM observations (Figure 5) are shown with chloride as counterion. Considering the duration of the GIXD experiments, two subphase concentrations were used, 1 and 10 $Zn^{2+}$ ions per BA molecule, in order to study the whole sequence of phases leading to the X-phase. Five stages are evidenced during $Zn^{2+}$ ions adsorption.

Stage 1: At a concentration of 1 $Zn^{2+}$ ion per BA molecule, the two lower-order diffraction peaks characteristic of the $L_{2h}$-phase are first evidenced, in the same way as over pure water. Figure 3a shows the diffraction pattern obtained at $t$ = 45 min. In the rectangular cell, the in-plane peak at $Q_{xy}$ = 1.455 $Å^{-1}$ corresponds to the (02) peak while the out-of-plane peak at $Q_{xy}$ = 1.483 $Å^{-1}$ is the degenerate $(11)/(1\bar{1})$ Bragg reflection. BA molecules are tilted toward a nearest-neighbor with an angle of


dx.doi.org/10.1021/jp407047a | J. Phys. Chem. B 2013, 117, 16275−16282

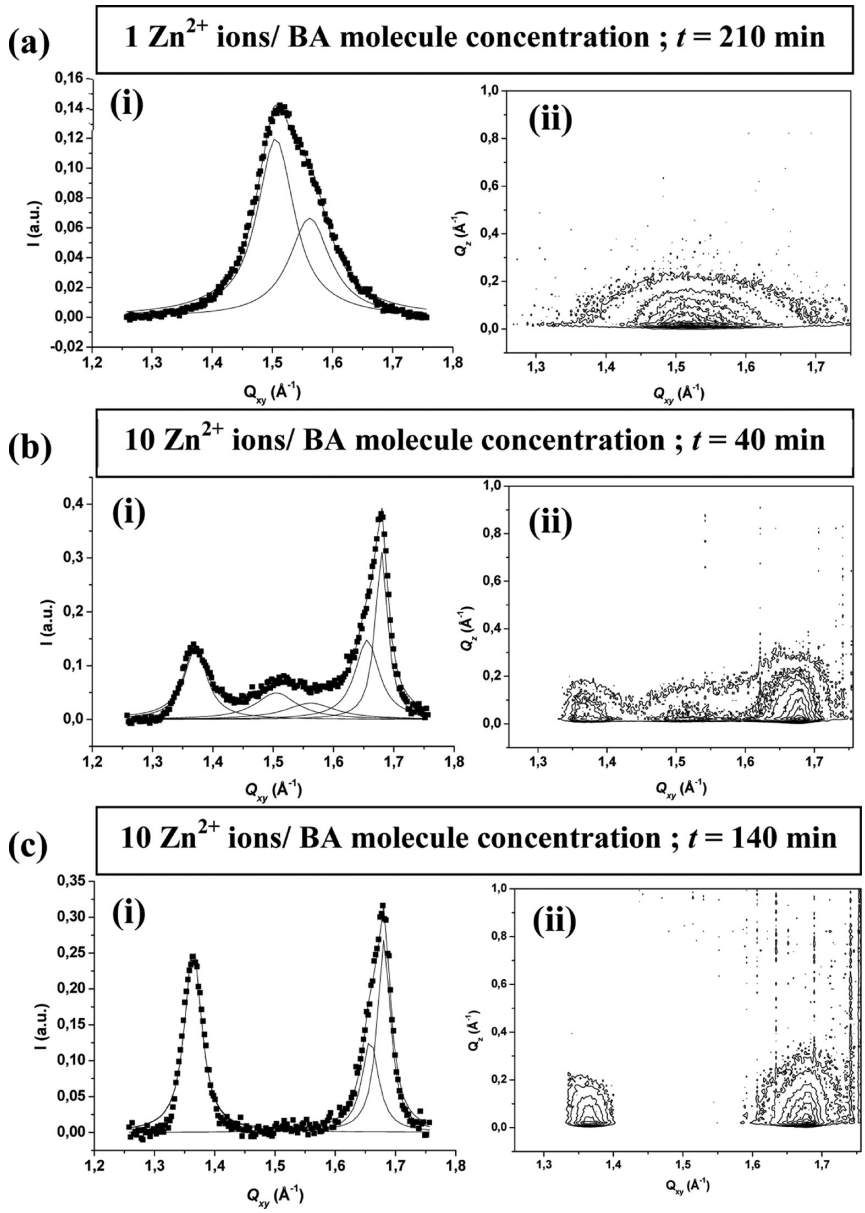


**Figure 4.** Evolution of the X-ray diffraction pattern with time obtained for a BA monolayer over a $ZnCl_2$ solution adjusted to pH 7.5. The surface pressure of the monolayer is $\Pi = 0$ mN/m. Scans of intensity as a function of $Q_{xy}$, integrated over $Q_z$ (i) and contours of equal intensity versus the in-plane and out-plane scattering vector components $Q_{xy}$ and $Q_z$ (ii) for (a) 1 $Zn^{2+}$ ions/BA molecule, $t$ = 210 min, I-phase; (b) 10 $Zn^{2+}$ ions/BA molecule, $t$ = 40 min, I–X′ phase coexistence; (c) 10 $Zn^{2+}$ ions/BA molecule, $t$ = 140 min, X′-phase.

about 21° with respect to the surface normal. By BAM with an analyzer on the path of the reflected light, different shades of gray corresponding to different tilt-azimuthal orientations of the molecules can be observed in the large domains of the $L_{2h}$-phase (Figure 5a) in the same way as over pure water at zero surface pressure. Then the diffraction spectra indicate that the tilt angle of the BA molecules decreases from 21° at $t$ = 45 min to about 15° at $t$ = 75 min. By means of BAM, a decrease in contrast between the regions of different tilt-azimuthal orientations is observed, in agreement with the tilt angle evolution (Figure 5b).

Stage 2: From $t$ = 75 min, a broad in-plane peak is detected in coexistence with the two $L_{2h}$-phase peaks, indicating a first-order phase transition. The scans obtained at $t$ = 115 min and shown in Figure 3b illustrate this transition. Figure 3b-i shows the X-ray scattered intensity spectrum as a function of $Q_{xy}$ integrated over all $Q_z$ values. In Figure 3b-ii showing contours of equal intensity as a function of $Q_{xy}$ and $Q_z$, it can be evidenced that the detected broad in-plane peak has the same $Q_{xy}$ position ($Q_{xy}$ = 1.518 Å$^{-1}$) as the (11)/(1$\bar{1}$) $L_{2h}$-phase peak. The rod scan of intensity at this $Q_{xy}$ position as a function of $Q_z$ is showed in Figure 3b-iii and supports the coexistence of these two peaks. During this stage, the positions of the three diffraction peaks remain fixed and only their intensity varies. Indeed, the intensity of the broad in-plane peak intensity increases while that of the $L_{2h}$-phase peaks decreases, as expected for a first-order phase transition. As shown in Figure 3c, the $L_{2h}$-phase is no longer visible at $t$ = 170 min and only the broad in-plane peak is observed at $Q_{xy}$ = 1.518 Å$^{-1}$. This peak corresponds to straight BA molecules organized in a hexagonal lattice. The rectangular cell parameters deduced from the peak position are $a$ = 4.78 Å and $b$ = 8.28 Å. The positional


dx.doi.org/10.1021/jp407047a | J. Phys. Chem. B 2013, 117, 16275−16282

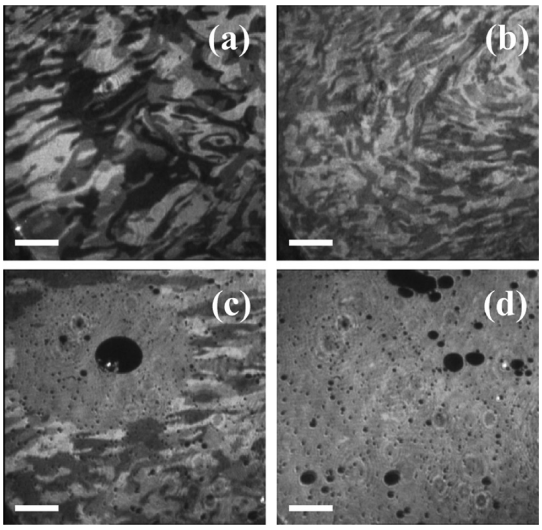


**Figure 5.** BAM images obtained with an analyzer for a BA monolayer spread over a $ZnCl_2$ solution of 1 $Zn^{2+}$ ions/BA molecule concentration, adjusted to pH 7.5. The surface pressure of the monolayer is $\Pi = 0$ mN/m. These images correspond to the following different times: (a) $t = 35$ min, $L_{2h}$-phase, (b) $t = 70$ min, $L_{2h}$-phase, (c) $t = 115$ min, $L_{2h}$−I phase transition, and (d) $t = 190$ min, I-phase. The white bar represents 100 $\mu$m.

correlation length $L$ is close to 50 Å, that is, only about 10 molecules. This phase strongly looks like the intermediate I-structure evidenced during adsorption of $Cd^{2+}$ or $Mg^{2+}$ ions under a BA monolayer.[12,13] Because $Cd^{2+}$ and $Mg^{2+}$ are known to induce superstructure formation and as this I-phase was not observed during $Cu^{2+}$ adsorption, we considered at first sight that the sequence of phases should be only related to the final state. However, these results show that even though $Cu^{2+}$ and $Zn^{2+}$ lead to the same organic X-phase structure without any ion ordering, the phases' sequence is strongly different.

BAM observations reveal at the beginning of this stage the nucleation of an optically isotropic phase in the condensed domains (Figure 5c), in agreement with the I-phase hexagonal packing evidenced with GIXD. The surface occupied by these isotropic patches increases at the expense of the $L_{2h}$-phase. At $t$ = 170 min, the condensed domains appear uniformly optically isotropic confirming the end of the first-order phase transition (Figure 5d). One can also notice the formation of gaseous holes indicating the monolayer condensation, in agreement with the decrease in molecular area from $A = 20.9$ Å$^2$ in the $L_{2h}$-phase to $A = 19.8$ Å$^2$ in the I-phase.

Stage 3: From $t = 170$ min, the shape of the I-phase peak does not remain symmetrical as shown on the scan obtained at $t = 210$ min (Figure 4a). Similar observations have been reported in the presence of $Cd^{2+}$ and $Mg^{2+}$ ions.[13,12]

Stage 4: The next stage of the kinetic process was followed for a $ZnCl_2$ solution 10 $Zn^{2+}$ ions per BA molecule. At $t = 40$ min, the diffraction pattern reveals a new phase coexistence. Indeed, two in-plane diffraction peaks, one of them being asymmetrical, are detected in addition to the broad asymmetrical peak associated to the intermediate I-phase (Figure 4b). For this new phase, one of the peak is located at $Q_{xy}$ = 1.363 Å$^{-1}$ while the asymmetrical peak is fitted by two peaks at $Q_{xy}$ = 1.658 Å$^{-1}$and $Q_{xy}$ = 1.680 Å$^{-1}$. The positions of two of the peaks ($Q_{xy}$ = 1.363 Å$^{-1}$, $Q_{xy}$ = 1.680 Å$^{-1}$) exactly correspond to those of the X-phase. This structure thus differs only from the X-phase by the asymmetry of the peak located at higher $Q_{xy}$. It will be called X′. Then, as expected for a first-order phase transition, the positions of the diffraction peaks remain fixed during this stage while the intensity of the I-phase peaks decreases with respect to the one of the X′-structure peaks. Finally, at $t = 140$ min only the peaks corresponding to the X′-structure are observed (Figure 4c). By means of BAM with analyzer, the I-phase and the X′-structure appear both optically isotropic, in the same way as the X-phase. Only the first-order $L_{2h}$−I phase transition can be thus observed.

Stage 5: The X′-structure continuously evolves toward the X-phase. Indeed, the peak at $Q_{xy}$ = 1.660 Å$^{-1}$ shifts toward the peak located at $Q_{xy}$ = 1.680 Å$^{-1}$, until a symmetrical peak at $Q_{xy}$ = 1.680 Å$^{-1}$ is obtained. From $t = 220$ min, the two characteristic peaks of the X-phase are observed. A second order X′−X phase transition is thus detected.

The main result is that divalent cations cannot be only classified according to the organic−inorganic structure formed above the concentration threshold but also with respect to the formation stages of this structure. Table 1 summarizes the final structure and the sequence of phases obtained in the presence of different cations.

First, considering the final structure, one can observe that van der Waals radii of $Cu^{2+}$ and $Zn^{2+}$cations (1.40 and 1.39 Å, respectively) which lead to the organic X-phase are smaller than those of $Mg^{2+}$ or $Cd^{2+}$ that form superstructures (1.73 and 1.58 Å, respectively). In the same way, the second hydration shell of $Cu^{2+}$ and $Zn^{2+}$ cations (408 and 395 pm, respectively) is smaller than that of $Mg^{2+}$ or $Cd^{2+}$ (431 and 420 pm, respectively).[25] However, little data are available on the nature of hydrolysis products formed in the presence of a fatty acid monolayer. To our knowledge, XAFS experiments have only been conducted for $Zn^{2+}$ ions adsorbed under a stearic acid monolayer at 0 °C or $Pb^{2+}$ ions adsorbed under a heneicosanoic acid monolayer at 9 °C.[19,26] In the case of $Zn^{2+}$ ions, the coordination number has been estimated to be 4 compared with 6 in the absence of monolayer. This indicates the strong influence of the monolayer on the hydrolysis products formed at the interface however in this case, no structural study of the organic−inorganic film was associated.

Second, comparing kinetic processes, one can notice that in the presence of $Zn^{2+}$ ions, the $L_{2h}$-phase evolves toward the X-phase through the new intermediate weakly ordered I-structure detected during the adsorption of $Mg^{2+}$ and $Cd^{2+}$ that form superstructures. The same organic I-structure is thus observed during $Zn^{2+}$, $Mg^{2+}$, and $Cd^{2+}$ cations adsorption nevertheless the self-organization of the cations in the final state does not take place in the case of $Zn^{2+}$ ions. Considering that adsorbed species are more likely hydrolysis products and that the intermediate I-phase could be a stage corresponding to their formation,[10,12,19] the difference observed between $Zn^{2+}$ and $Mg^{2+}$ or $Cd^{2+}$ could be related to complexes lability. $Mg^{2+}$ or $Cd^{2+}$ complexes could be less stable than $Zn^{2+}$ complexes leading to their association to carboxylic headgroups, that is, to superstructure formation. Then comparing $Cu^{2+}$ and $Zn^{2+}$ cations that lead to the same final structure, we evidenced a drastically different kinetic evolution toward the X-phase. Indeed, no transient I-structure is evidenced in presence of $Cu^{2+}$ ions.[15] Nevertheless in both cases, an X-like structure is evidenced that evolves through a second order phase transition toward the X-phase. These results show that kinetic studies can bring new information on these systems.


dx.doi.org/10.1021/jp407047a | J. Phys. Chem. B 2013, 117, 16275−16282

## IV. CONCLUSION

The structure of BA monolayers spread over salt solutions of zinc was investigated at two subphase pHs (5.5 and 7.5) and in the presence of different counterions. At pH 5.5, $Zn^{2+}$ ions have just a condensing effect on the BA monolayer without any change with respect to the phase transitions detected over pure water. At pH 7.5, the X-phase is formed immediately at room temperature above a concentration threshold independent of the counterion. Second order peaks were detected for the first time, confirming the peaks indexation. Below the threshold, the kinetic evolution is independent of the counterion. The $L_{2h}$-phase evolves to the X-phase through two first-order and one second-order phase transitions, with the sequence of phases $L_{2h}$−I−X′−X. The I-phase is the new weakly ordered intermediate structure previously evidenced during the adsorption of $Mg^{2+}$ and $Cd^{2+}$ that induce superstructures. The X′-structure is very close to the one of the X-phase nevertheless the unit cell distortion is less pronounced. These results indicate that the divalent cations cannot be only classified according to the final structure since $Cu^{2+}$ and $Zn^{2+}$ both lead to the fatty acid X-phase formation, however through significantly different kinetic processes. Finally, any effect of the counterion is evidenced neither during the kinetic process nor in the final state. In order to improve the understanding of headgroup-cation interactions, further studies are in progress regarding the adsorption kinetics of other divalent cations.

## AUTHOR INFORMATION

### Corresponding Author

*E-mail: Sophie.Cantin-Riviere@u-cergy.fr. Phone: +33-1-34-25-70-06. Fax: +33-1-34-25-70-71.

### Notes

The authors declare no competing financial interest.

## REFERENCES

(1) Tang, Z.; Kotov, N. A.; Magonov, S.; Ozturk, B. Nanostructured artificial nacre. *Nat. Mater.* **2003**, *2*, 413−418.

(2) Kmetko, J.; Yu, C.; Evmenenko, G.; Kewalramani, S.; Dutta, P. Organic-template-directed nucleation of strontium fluoride and barium fluoride: Epitaxy and strain. *Phys. Rev. B* **2003**, *68*, 085415.

(3) Leveiller, F.; Bohm, C.; Jacquemain, D.; Mohwald, H.; Leiserowitz, L.; Kjaer, K.; Als-Nielsen, J. Two-Dimensional Crystal Structure of Cadmium Arachidate Studied by Synchrotron X-ray Diffraction and Reflectivity. *Langmuir* **1994**, *10*, 819−829.

(4) Lendrum, C.; McGrath, K. M. Toward Controlled Nucleation: Balancing Monolayer Chemistry with Monolayer Fluidity. *Cryst. Growth Des.* **2010**, *10*, 4463−4470.

(5) Stripe, B.; Uysal, A.; Lin, B.; Meron, M.; Dutta, P. Charge, Stereochemistry or Epitaxy? Toward Controlled Biomimetic Nucleation at Mixed Monolayer Templates. *Langmuir* **2012**, *28*, 572−578.

(6) Kewalramani, S.; Kim, K.; Stripe, B.; Evmenenko, G.; Dommett, G. H. B.; Dutta, P. Observation of an Organic-Inorganic Lattice Match during Biomimetic Growth of (001)-Oriented Calcite Crystals under Floating Sulfate Monolayers. *Langmuir* **2008**, *24*, 10579−10582.

(7) He, J. X.; Yamashita, S.; Jones, W.; Yamagishi, A. Templating Effects of Stearate Monolayer on Formation of Mg-Al-Hydrotalcite. *Langmuir* **2002**, *18*, 1580−1586.

(8) Weissbuch, I.; Buller, R.; Kjaer, K.; Als-Nielsen, J.; Leiserowitz, L.; Lahav, M. Crystalline self-assembly of organic molecules with metal ions at the air−aqueous solution interface. A grazing incidence X-ray scattering study. *Colloids Surf., A* **2002**, *208*, 3−27.

(9) Kmetko, J.; Datta, A.; Evmenenko, G.; Dutta, P. The Effect of Divalent Ions on Langmuir Monolayer and Subphase Structure. *J. Phys. Chem. B* **2001**, *105*, 10818−10825.

(10) Kmetko, J.; Datta, A.; Evmenenko, G.; Durbin, M. K.; Richter, A. G.; Dutta, P. Ordering in the Subphase of a Langmuir Monolayer: X-ray Diffraction and Anomalous Scattering Studies. *Langmuir* **2001**, *17*, 4697−4700.

(11) Cantin, S.; Pignat, J.; Daillant, J.; Perrot, F.; Konovalov, O. Grazing incidence X-ray diffraction determination of the structure of two-dimensional organic-inorganic crystals at the water surface. *Soft Matter* **2010**, *6*, 1923.

(12) Cantin, S.; Pignat, J.; Perrot, F.; Fontaine, P.; Goldmann, M. Observation of a two-step mechanism in the formation of a superstructure of cadmium-behenic acid Langmuir monolayer: evidence of an intermediate structure. *Phys. Rev. E* **2004**, *70*, 050601(R).

(13) Pignat, J.; Cantin, S.; Liu, R. C. W.; Goldmann, M.; Fontaine, P.; Daillant, J.; Perrot, F. pH dependent kinetics of MgCl2 adsorption under a fatty acid monolayer. *Eur. Phys. J. E* **2006**, *20*, 387.

(14) Shih, M. C.; Bohanon, T. M.; Mikrut, J. M.; Zschack, P.; Dutta, P. Pressure and pH dependence of the structure of a fatty acid monolayer with calcium ions in the subphase. *J. Chem. Phys.* **1992**, *96*, 1556−1559.

(15) Cantin, S.; Péralta, S.; Fontaine, P.; Goldmann, M.; Perrot, F. Evolution toward the X Phase of Fatty Acid Langmuir Monolayers on a Divalent Cation Solution. *Langmuir* **2010**, *26*, 830.

(16) Datta, A.; Kmetko, J.; Yu, C.-J.; Richter, A. G.; Chung, K.-S.; Bai, J.-M.; Dutta, P. pH-Dependent Appearance of Chiral Structure in a Langmuir Monolayer. *J. Phys. Chem. B* **2000**, *104*, 5797−5802.

(17) Le Calvez, E.; Blaudez, D.; Buffeteau, T.; Desbat, B. Effect of Cations on the Dissociation of Arachidic Acid Monolayers on Water Studied by Polarization-Modulated Infrared Reflection-Absorption Spectroscopy. *Langmuir* **2001**, *17*, 670−674.

(18) Bloch, J. M.; Yun, W. Condensation of monovalent and divalent metal ions on a Langmuir monolayer. *Phys. Rev. A* **1990**, *41*, 844−862.

(19) Boyanov, M. I.; Kmetko, J.; Shibata, T.; Datta, A.; Dutta, P.; Bunker, B. A. Mechanism of Pb Adsorption to Fatty Acid Langmuir Monolayers Studied by X-ray Absorption Fine Structure Spectroscopy. *J. Phys. Chem. B* **2003**, *107*, 9780−9788.

(20) Hénon, S.; Meunier, J. Microscope at the Brewster angle: Direct observation of first-order phase transitions in monolayers. *Rev. Sci. Instrum.* **1991**, *62*, 936−939.

(21) Fradin, C.; Daillant, J.; Braslau, A.; Luzet, D.; Alba, M.; Goldmann, M. Microscopic measurement of the linear compressibilities of two-dimensional fatty acid mesophases. *Eur. Phys. J. B* **1998**, *1*, 57−69.

(22) Vollhardt, D.; Fainerman, D. B. Review progress in characterization of Langmuir monolayers by consideration of compressibility. Adv. *Colloid Interface Sci.* **2006**, *127*, 83−97.

(23) Kuzmenko, I.; Kaganer, V. M.; Leiserowitz, L. Packing of Hydrocarbon Chains and Symmetry of Condensed Phases in Langmuir Monolayers. *Langmuir* **1998**, *14*, 3882−3888.

(24) Kundu, S.; Langevin, D. Fatty acid monolayer dissociation and collapse: effect of pH and cations. *Colloids Surf., A* **2008**, *325*, 81−85.

(25) Ohtaki, H.; Radnai, T. Structure and Dynamics of Hydrated Ions. *Chem. Rev.* **1993**, *93*, 1157−1204.

(26) Watanabe, I.; Tanida, H.; Kawauchi, S. Coordination Structure of Zinc(II) Ions on a Langmuir Monolayer, Observed by Total-Reflection X-ray Absorption Fine Structure. *J. Am. Chem. Soc.* **1997**, *119*, 12018−12019.